JBC RESEARCH ARTICLE

The G4 resolvase RHAU regulates ventricular trabeculation and compaction through transcriptional and post-transcriptional mechanisms

Received for publication, October 7, 2021, and in revised form, November 16, 2021 Published, Papers in Press, November 25, 2021,
https://doi.org/10.1016/j.jbc.2021.101449

Xinyi Huang[1], **Ke Zhao**[1], **Mingyang Jiang**[1], **Dehui Qiu**[2], **Jun Zhou**[2], **and Zhongzhou Yang**[1,*]

From the [1]*State Key Laboratory of Pharmaceutical Biotechnology, MOE Key Laboratory of Model Animal for Disease Study, Model Animal Research Center, and Jiangsu Key Laboratory of Molecular Medicine, Nanjing University Medical School, Nanjing, China;* [2]*State Key Laboratory of Analytical Chemistry for Life Science, School of Chemistry & Chemical Engineering, Nanjing University, Nanjing, China*

Edited by Ronald Wek

The G-quadruplex (G4) resolvase RNA helicase associated with AU-rich element (RHAU) possesses the ability to unwind G4 structures in both DNA and RNA molecules. Previously, we revealed that RHAU plays a critical role in embryonic heart development and postnatal heart function through modulating mRNA translation and stability. However, whether RHAU functions to resolve DNA G4 in the regulation of cardiac physiology is still elusive. Here, we identified a phenotype of noncompaction cardiomyopathy in cardiomyocyte-specific *Rhau* deletion mice, including such symptoms as spongiform cardiomyopathy, heart dilation, and death at young ages. We also observed reduced cardiomyocyte proliferation and advanced sarcomere maturation in *Rhau* mutant mice. Further studies demonstrated that RHAU regulates the expression levels of several genes associated with ventricular trabeculation and compaction, including the *Nkx2-5* and *Hey2* that encode cardiac transcription factors of NKX2-5 and Hey2, and the myosin heavy chain 7 (*Myh7*) whose protein product is MYH7. While RHAU modulates *Nkx2-5* mRNA and *Hey2* mRNA at the post-transcriptional level, we uncovered that RHAU facilitates the transcription of *Myh7* through unwinding of the G4 structures in its promoter. These findings demonstrated that RHAU regulates ventricular chamber development through both transcriptional and post-transcriptional mechanisms. These results contribute to a knowledge base that will help to understand the pathogenesis of diseases such as noncompaction cardiomyopathy.

Noncompaction cardiomyopathy (NCC) is a genetically heterogeneous disorder with diverse clinical phenotypes, which has gained increased awareness and prevalence in both children and adults, perhaps because of advances in cardiovascular imaging (1, 2). Clinically, NCC manifests nine distinct subtypes, and all of them show the common characteristic of abnormal trabeculations in the left ventricle (LV) (2, 3).

NCC emerges from myocardial developmental defects as a consequence of impaired trabeculation or disrupted compaction or both of them during embryonic heart development (4). Initiation of ventricular trabeculation distinguishes the trabecular zone from adjacent compact zone (5, 6), and these two zones demonstrate regional-specific properties in cell proliferation and gene expression patterns (7, 8). For instance, the trabecular zone is featured by the expression of *Irx3*, *Bmp10*, *Cx40*, *Slit2*, *Etv1*, and *Sema3a*, whereas in the compact zone, *Hey2*, *Tbx20*, and *N-Myc* are specifically expressed (5, 9). In this respect, endocardial Notch signaling is required for the formation and maturation of both trabecular and compact myocardium (9, 10). Mutation of *Mib1*, a positive regulator of Notch signaling, has been identified in NCC patients, and animal model has confirmed Mib1 function in ventricular chamber development (11).

On the other hand, defective myofibrillogenesis (myofibril assembly) was proposed as a key pathogenic factor for NCC because mutation of the sarcomere genes of *Myh7*, *Mybpc3*, and *TTN* was frequently identified in NCC patients (12, 13). Interestingly, a recent study of compound heterozygosity for the single-nucleotide variants of *Myh7*, *Mkl2*, and *Nkx2-5* in mice recapitulated the human NCC phenotype (14). This study affirmed the contribution of *Myh7* mutation to incidence of NCC and revealed *Nkx2-5* variant as a genetic modifier (14). Nonetheless, one puzzling issue is that mutations of *Myh7* and *Nkx2-5* were also identified in other forms of cardiomyopathies including hypertrophic cardiomyopathy and dilated cardiomyopathy (13). Therefore, it is necessary and interesting to distinguish the action and contribution of *Myh7* and the modifier genes such as *Nkx2-5* in the occurrence of distinct cardiomyopathies.

G-quadruplex (G4) is a four-stranded tetrad structure resulting from stacking of G-quartets formed by four guanines *via* Hoogsteen base paring in a planar arrangement (15, 16). G4 structures are abundantly distributed in the genome and mRNA molecules, with preference in the areas of regulatory domains like promoters and transcription start sites, replication hot spots, and telomeres in the genome, and are enriched in the UTRs of mRNAs (15). Thus, G4 structures are involved in regulating transcription, DNA replication and telomere maintenance, and mRNA translation and stability (15, 16).

* For correspondence: Zhongzhou Yang, zhongzhouyang@nju.edu.cn.

RHAU (DHX36 and G4R1) is a resolvase/helicase to unwind the G4 structures in DNA and RNA (17–19). Previously, we demonstrated an essential function of RHAU in mouse embryonic heart development (20). Our recent work also revealed a pivotal role of RHAU in postnatal heart function (21). In these two studies, we have identified the mRNAs of *Nkx2-5*, *Yap1*, and *Hexim1* as RHAU regulatory targets, and RHAU promotes their translation through association with the G4 structures in the 5′-UTR of these mRNAs. Meanwhile, RHAU binds to the 3′-UTR of these mRNAs to facilitate mRNA decay (20, 21). While these results uncovered the critical function of RHAU as RNA G4 resolvase to modulate gene expression at post-transcriptional level, whether RHAU functions to resolve DNA G4 to regulate cardiac physiology is still elusive.

Deletion of *Rhau* in cardiac progenitors (using *Nkx2-5*-Cre or *Mesp1*-Cre) caused severe heart defects and embryonic lethality by E14.5, excluding study of ventricular chamber development in midterm (20). In an effort to extend the study of RHAU in late heart development, particularly in ventricular chamber formation, we deleted *Rhau* in embryonic cardiomyocytes (*via cTNT*-Cre–mediated excision) and identified the NCC phenotype. Furthermore, we have figured out that RHAU modulated gene expression level of several genes involved in ventricular trabeculation and compaction. In addition to the post-transcriptional mechanisms, RHAU controlled gene transcription through unwinding G4 structures in the genome (DNA) to govern ventricular chamber development. These findings demonstrated that RHAU regulates ventricular chamber formation through transcriptional and post-transcriptional mechanisms. Meanwhile, this study provided a valuable mouse model for understanding NCC.

Results

RHAU deficiency led to the phenotypes of NCC

We previously unveiled the essential function of RHAU in embryonic heart development of mouse (20). However, these cardiac progenitor-specific *Rhau*-deletion mice manifested severe heart defects and embryonic lethality by E14.5 with complete penetrance, which made it impossible to investigate the ventricular chamber formation during the period from midterm of gestation to birth.

To study the function of RHAU in the ventricular chamber formation, we first removed *Rhau* using *Mef2c-AHF*-Cre that showed Cre activity in both outflow tract and the right ventricle (RV) (22). The *Rhau$^{f/f}$;Mef2c-AHF-Cre* embryos could develop to term and be born, and the majority of these mice could survive up to 6 months (Fig. 1*A*). Gross analysis of *Rhau$^{f/f}$;Mef2c-AHF-Cre* and control mice (*Rhau$^{f/f}$* or *Rhau$^{f/+}$* littermates in this study) at postnatal 21 days (P21) displayed prominently enlarged hearts in *Rhau$^{f/f}$;Mef2c-AHF-Cre* mice compared with control (Fig. 1, *B* and *C*). Histological examination of heart tissues revealed dilated ventricle chamber, thinner myocardium wall, and sponge-like trabecula in the RV of *Rhau$^{f/f}$;Mef2c-AHF-Cre* mice, indicative of ventricular noncompaction (NCC) (Figs. 1, *D–G* and S1, *A* and *A*′).

Ventricular noncompaction is more frequent and harmful in the LV. To see whether RHAU deficiency in the LV could cause noncompaction as in the RV, we crossed *Rhau* floxed mice with *cTNT*-Cre (*Tnnt2*-Cre) mice that have Cre activity in the cardiomyocytes of both ventricles (23) to generate *Rhau$^{f/f}$;cTNT-Cre* mice. These mice could also develop to term but started to die several days after birth (Fig. 1*H*). We observed loss of nearly 80% of *Rhau$^{f/f}$;cTNT-Cre* mice by 2 months (Fig. 1*H*). Gross assessment of the hearts from P13 mice exhibited bigger size in *Rhau$^{f/f}$;cTNT-Cre* mice than in control (Fig. 1, *I* and *J*). Histological inspection disclosed spongiform cardiomyopathy, thinned ventricular wall, and chamber dilation in the LV of *Rhau$^{f/f}$;cTNT-Cre* mice (Figs. 1, *K–N* and S1, *B* and *B*′).

In addition, we asked question of whether losing RHAU activity in the endocardium had a contribution to ventricular noncompaction. We removed RHAU in the endocardial and endothelial cells of *Rhau$^{f/f}$;Tie2-Cre* mice and found normal embryonic development. A thorough investigation failed to observe a difference between the hearts of *Rhau$^{f/f}$;Tie2-Cre* and control mice (Fig. 1, *O* and *P*), suggesting that RHAU function was dispensable in the endocardium and endothelium.

Taken together, these data demonstrated that mice with RHAU deficiency in the embryonic cardiomyocytes truthfully recapitulated typical human NCC phenotypes.

Defective trabeculation and compaction in RHAU-deficient mice

To understand the NCC phenotype observed in postnatal *Rhau$^{f/f}$;cTNT-Cre* mice, we performed gross and histological analysis of embryonic heart. At E12.5, the hearts appeared comparable between the two groups (Fig. 2, *A* and *B*). However, substantially enlarged ventricles were noticed in the *Rhau$^{f/f}$;cTNT-Cre* mice compared with control at E14.5 (Fig. 2, *C* and *D*). Histological study of these hearts not only confirmed the ventricular dilation but also recognized thinned ventricular wall in the heart of *Rhau$^{f/f}$;cTNT-Cre* mice at E14.5 (Fig. 2, *E*, *F*, *E*′, and *F*′). The ventricles were more dilated in the *Rhau$^{f/f}$;cTNT-Cre* mice at E16.5 than at E14.5 (Fig. 2, *G*, *H*, *G*′, *H*′, and *I*).

In addition, significantly elevated trabeculation was detected in the ventricles of *Rhau$^{f/f}$;cTNT-Cre* mice at E14.5 (Fig. 2, *E*, *F*, *E*′, and *F*′). Quantitative examination of the area of trabecular and compact zone showed an increased ratio of trabecular area/compact area in the *Rhau$^{f/f}$;cTNT-Cre* mice compared with control at E14.5, and the number of this ratio was more than doubled in the *Rhau$^{f/f}$;cTNT-Cre* mice compared with control at E16.5 (Fig. 2*J*). Moreover, the trabeculae of *Rhau$^{f/f}$;cTNT-Cre* mice was thicker than control mice at E14.5 (Fig. 2*K*).

Gross and histological analysis were also performed with the embryonic heart of *Rhau$^{f/f}$;Mef2c-AHF-Cre* mice. Ventricular dilation and thickened trabeculae in the RV were noticed (Fig. S1, *C–N*).

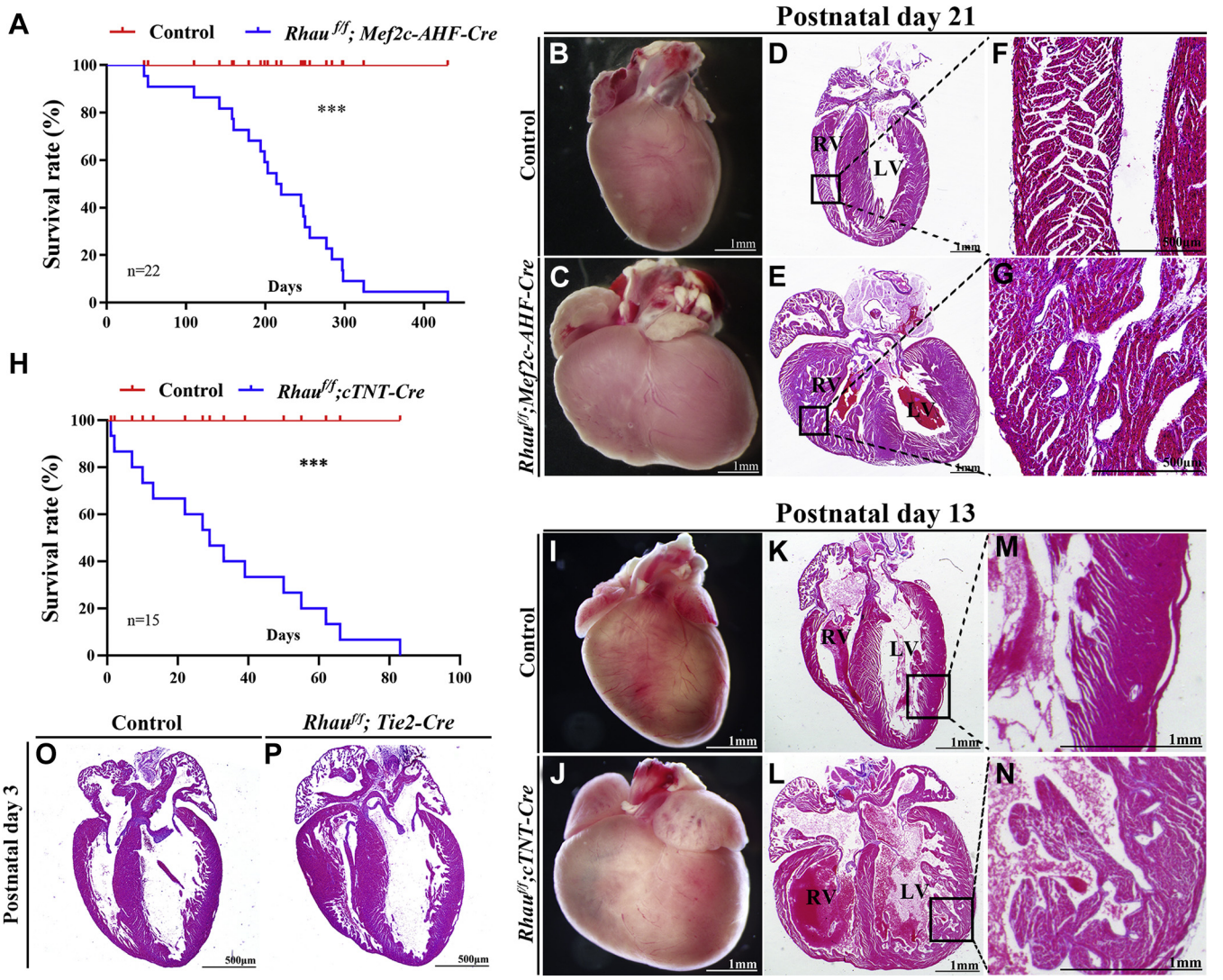

Figure 1. RHAU deficiency recapitulated the phenotypes of human NCC. *A*, survival curves of control and *Rhau*$^{f/f}$*;Mef2c-AHF-Cre* mice. N = 22 for control mice and N = 22 for *Rhau*$^{f/f}$*;Mef2c-AHF-Cre* mice. $p < 0.001$ (***). *B* and *C*, gross analysis of the hearts from control and *Rhau*$^{f/f}$*;Mef2c-AHF-Cre* mice at P21. The RV was remarkably enlarged in the *Rhau* mutant mice. The scale bars represent 1 mm. *D* and *E*, histological analysis of the heart at P21. The RV displayed spongiform cardiomyopathy in the *Rhau* mutant mice. The scale bars represent 1 mm. *F* and *G*, higher magnification of the *boxed areas* in (*D*) and (*E*). The scale bars represent 500 μm. *H*, survival curves of control and *Rhau*$^{f/f}$*;cTNT-Cre* mice. N = 15 for control mice and N = 15 for *Rhau*$^{f/f}$*;cTNT-Cre* mice. $p < 0.001$ (***). *I* and *J*, gross analysis of heart from control and *Rhau*$^{f/f}$*;cTNT-Cre* mice at P13. The scale bars represent 1 mm. *K* and *L*, histological analysis of the heart at P13. The scale bars represent 1 mm. *M* and *N*, higher magnification of the *boxed areas* in (*K*) and (*L*). The LV displayed spongiform cardiomyopathy in the *Rhau* mutant mice. The scale bars represent 1 mm. *O* and *P*, histological analysis of heart in control and *Rhau*$^{f/f}$*;Tie2-Cre* mice at P3. The scale bars represent 200 μm. Control mice were *Rhau*$^{f/f}$ or *Rhau*$^{f/+}$ littermates. LV, left ventricle; NCC, noncompaction cardiomyopathy; RHAU, RNA helicase associated with AU-rich element; RV, right ventricle.

Collectively, these results demonstrated enhanced trabeculation with thickened trabeculae in the *Rhau* mutant mice.

Reduced cardiomyocyte proliferation and advanced sarcomere maturation in Rhau *mutant mice*

Cell proliferation of the ventricular cardiomyocytes was considered as a crucial element contributing to NCC, and both reduced and enhanced *Bmp10* expression level were recorded in impacting cardiomyocyte proliferation in NCC mouse models (11, 24, 25). We found that the proliferation activity of the cardiomyocytes was reduced in *Rhau*$^{f/f}$*;Mef2c-AHF-Cre* mice at both E12.5 and E14.5 compared with control (Fig. S2, *A* and *B*). We therefore examined the cell proliferation status of the ventricular cardiomyocytes by immunofluorescence (IF) staining. The results demonstrated that the number of Ki-67^{+} cardiomyocytes was dramatically decreased in the ventricles of *Rhau*$^{f/f}$*;cTNT-Cre* mice at both E12.5 and E14.5, and there was no big difference between the two ventricles (Figs. 3, *A–E* and S2, *C* and *D*). In addition, *Rhau* deletion had little effect on the proliferative activity of endocardial cells (Fig. S2, *E* and *F*). Examination of *Bmp10* expression level disclosed a slight reduction in the heart tissues of *Rhau*$^{f/f}$*;cTNT-Cre* mice (Fig. S3*A*).

In addition, cell apoptosis of cardiomyocytes was assessed by TUNEL staining, and no statistically significant difference was found between the control and *Rhau*$^{f/f}$*;cTNT-Cre* mice at E12.5 and E14.5 (Figs. 3, *F–H* and S2, *G–I*). However,

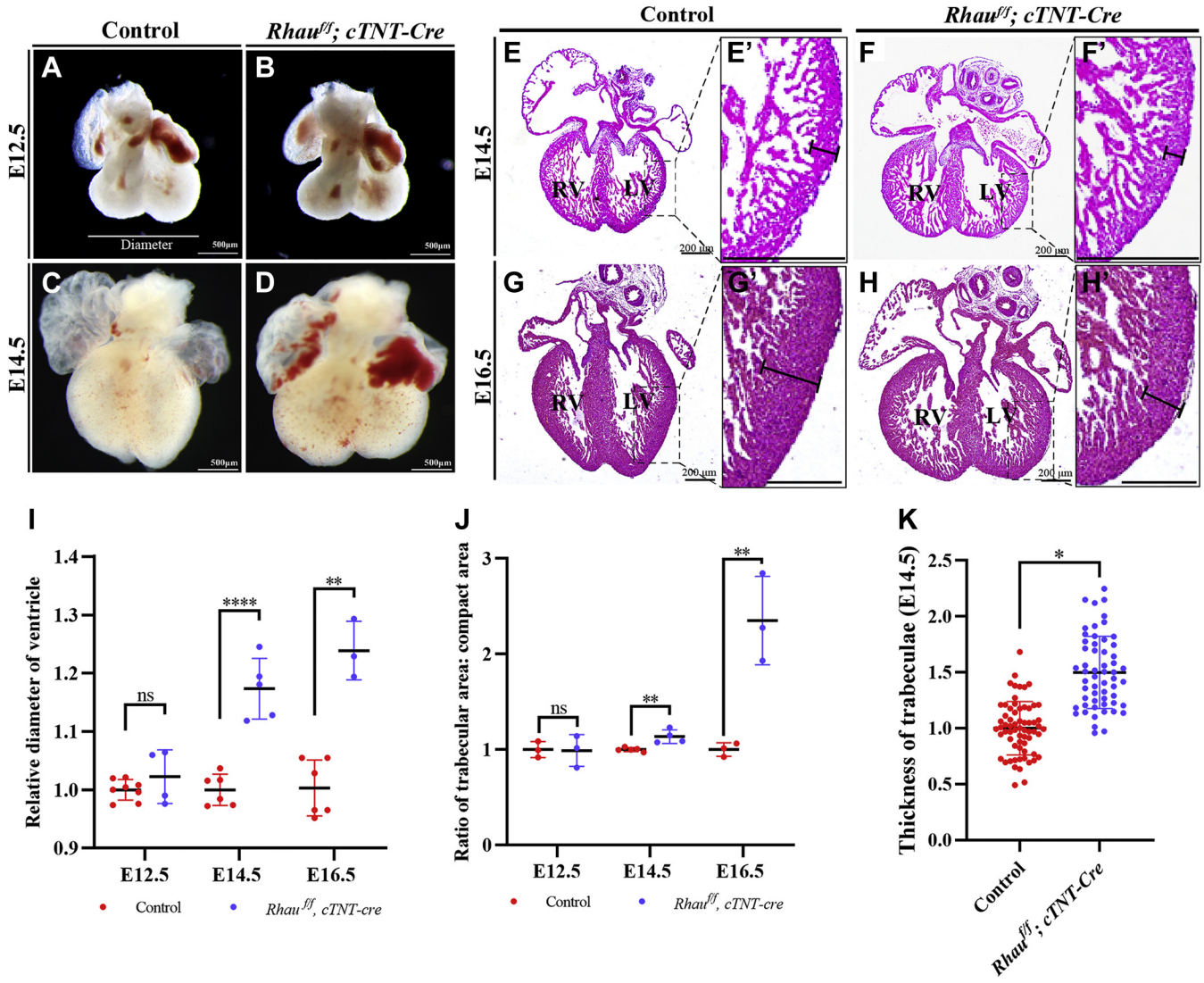

Figure 2. Defective trabeculation and compaction in RHAU-deficient mice. *A–D*, gross analysis of the hearts from control and *Rhau*$^{f/f}$;*cTNT-Cre* mice at E12.5 and E14.5. The ventricles were larger in the *Rhau* mutant mice than in control at E14.5. The scale bars represent 500 μm. *E–H*, histological analysis of the hearts in control and *Rhau*$^{f/f}$;*cTNT-Cre* mice at E14.5 and E16.5. The scale bars represent 200 μm. *E′–H′*, higher magnification of the *boxed areas* in (*E–H*). Thicker trabeculae and thinner ventricular compact zones were observed in the *Rhau* mutant mice. The scale bars represent 50 μm. *I*, quantification of the diameter of ventricles in (*A–D*). The *Rhau* mutants showed increased diameter of ventricles at E12.5, E14.5, and E16.5. Control mice: E12.5 (N = 8), E14.5 (N = 6), and E16.5 (N = 6). *Rhau*$^{f/f}$;*cTNT-Cre* mice: E12.5 (N = 4), E14.5 (N = 5), and E16.5 (N = 3). $p > 0.05$ (ns), $p < 0.01$ (**), and $p < 0.0001$ (****). *J*, ratio of trabecular area to compact area in (*E–H*). The ratio was increased in *Rhau*$^{f/f}$;*cTNT-Cre* mice at E12.5, E14.5, and E16.5 compared with control. Control mice: E12.5 (N = 3), E14.5 (N = 5), and E16.5 (N = 3). *Rhau*$^{f/f}$;*cTNT-Cre* mice: E12.5 (N = 3), E14.5 (N = 4), and E16.5 (N = 3). $p > 0.05$ (ns), $p < 0.01$ (**). *K*, quantification of the trabeculae thickness at E14.5. N = 4 for control mice and N = 4 for *Rhau*$^{f/f}$;*cTNT-Cre* mice. $p < 0.05$ (*). Control mice were *Rhau*$^{f/f}$ or *Rhau*$^{f/+}$ littermates. LV, left ventricle; ns, nonsignificant; RHAU, RNA helicase associated with AU-rich element; RV, right ventricle.

quantification analysis of the cardiomyocyte numbers in the ventricle at E14.5 revealed a significant reduction in the *Rhau*$^{f/f}$;*cTNT-Cre* mice compared with control mice at E14.5 (Fig. S2*J*).

From E12.5, ventricular cardiomyocytes start the process of maturation, and sarcomere growth is one of the features of cardiomyocyte maturation (26). We first checked the sarcomere structure in the cardiomyocytes of control and *Rhau*$^{f/f}$;*cTNT-Cre* mice at E12.5 and E14.5 by IF staining for α-actinin, and the results showed comparable patterns between the two groups at these developmental stages (Fig. 4, *A–D*). We also checked the structure of myofibrils of the LV and RV at both E12.5 and E14.5 through IF staining and failed to detect an obvious difference between control and *Rhau* mutant mice (Fig. S3, *B* and *C*). However, ultrastructural examination of the sarcomere by transmission electron microscopy displayed alterations with sarcomere length and thickness between these two groups (Fig. 4, *E–L*). The distance of two Z-lines was defined as sarcomere length, and the length of single Z-line was regarded as sarcomere thickness. From E12.5 to E14.5, the average sarcomere length in the cardiomyocytes of both trabecular and compact zone increased prominently in the control mice, indicating sarcomere growth (Fig. 4, *M* and *N*). In the *Rhau*$^{f/f}$;*cTNT-Cre* mice, we observed that the average sarcomere length in the trabecular cardiomyocytes at E12.5 was remarkably increased

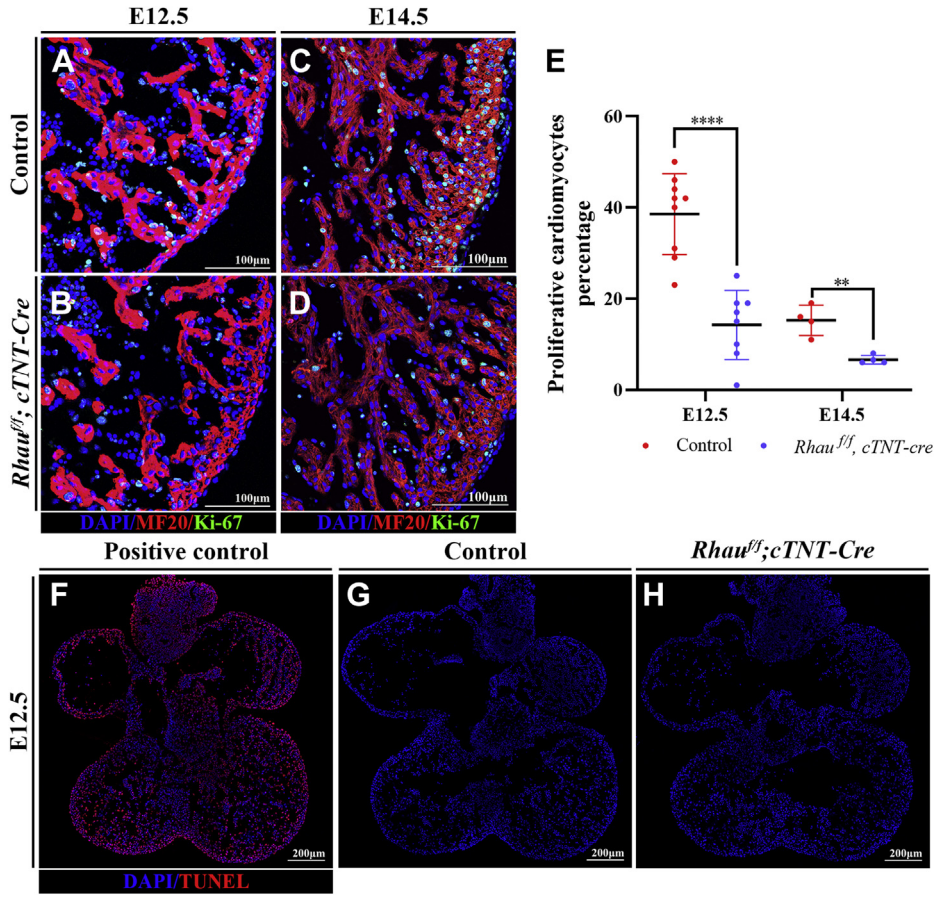

Figure 3. Reduced cardiomyocyte proliferation in *Rhau* mutant mice. *A–D*, IF staining for Ki-67 in heart sections at E12.5 and E14.5. MF20 stained cardiomyocytes (in *red*), and Ki-67 stained proliferative cells (in *green*). The nuclei were stained by DAPI (in *blue*). MF20$^+$ and Ki-67$^+$ double positive cells represented proliferative cardiomyocytes. The scale bars represent 100 μm. *E*, the percentage of proliferative cardiomyocytes. Significantly reduced proliferative activity of cardiomyocytes was detected in the *Rhau* mutant heart at E12.5 and E14.5. Control mice: E12.5 (N = 9) and E14.5 (N = 4). *Rhau$^{f/f}$;cTNT-Cre* mice: E12.5 (N = 8) and E14.5 (N = 4). $p < 0.01$ (**), $p < 0.0001$ (****). *F–H*, TUNEL staining in the heart sections at E12.5. The section in (*F*) was treated with DNase I as the positive control. TUNEL signal was in *red*, and nucleus was stained by DAPI (in *blue*). The scale bars represent 200 μm. Control mice were *Rhau$^{f/f}$* or *Rhau$^{f/+}$* littermates. DAPI, 4′,6-diamidino-2-phenylindol; IF, immunofluorescence.

and nearly reached the sarcomere length in the cardiomyocytes of control mice at E14.5 (Fig. 4*M*). The average sarcomere length in the cardiomyocytes of compact zone of the *Rhau$^{f/f}$;cTNT-Cre* mice was also enlarged compared with control at E12.5 but exhibited a slightly shorter status than control at E14.5 (Fig. 4*N*). As for the sarcomere thickness, it was bigger in the trabecular cardiomyocytes of the *Rhau$^{f/f}$;cTNT-Cre* mice at E12.5 than control (Fig. 4*O*). At both E12.5 and E14.5, the sarcomeres in the compact cardiomyocytes of the *Rhau$^{f/f}$;cTNT-Cre* mice were thicker than control (Fig. 4*P*). To summarize these changes, the sarcomeres in the trabecular zone of *Rhau* mutant mice increased fast in length and thickness by E12.5 and kept in a quiescent state by E14.5 when they were thicker than those in control mice. While in the compact zone, the sarcomeres became longer and thinner from E12.5 to E14.5 in control mice, those in the *Rhau* mutant mice stopped changes and were shorter and thicker than control by E14.5. In addition, the sarcomeres in the *Rhau* mutant mice failed to change (length and thickness) in either trabecular or compact zone between E12.5 and E14.5, suggesting a terminal maturation status. These changes with the sarcomeres, especially the increased sarcomere length and thickness by E12.5, indicated advanced maturation in the cardiomyocytes of *Rhau* mutant mice.

Altered expression pattern of NCC-associated genes in Rhau *mutant heart*

Our previous studies have uncovered a post-transcriptional regulatory mechanism by RHAU in modulating mRNA stability and translation. Through binding to the 3′-UTR of target mRNAs, RHAU facilitated mRNA degradation. Upon removal of RHAU, the levels of the target mRNAs were enhanced tremendously. Therefore, we performed RNA-Seq analysis to search for potential target genes with increased levels in the *Rhau* mutant heart, and the initial RNA-Seq results were shown in the heat map (Fig. S3*D*). Examination of the core components (*Jag1*, *Jag2*, and *Mib1*) in the Notch signaling pathway failed to find a big difference between control and *Rhau$^{f/f}$;cTNT-Cre* mice (Fig. S3*E*).

A detailed analysis of the RNA-Seq data identified the NCC-associated genes with upregulated or downregulated expression levels (Fig. 5*A*). In the upregulated genes, the cardiac-specific transcription factor *Nkx2-5* mRNA was

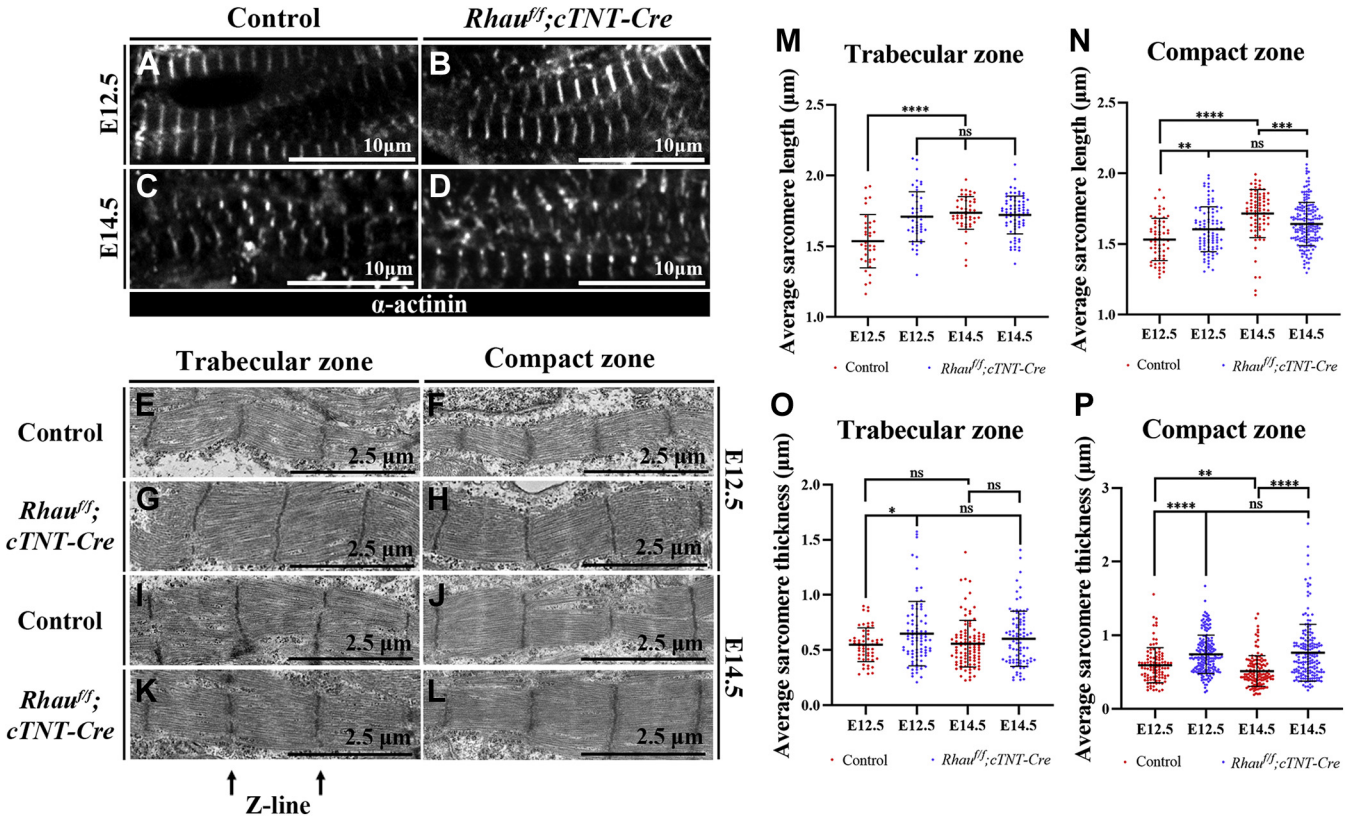

Figure 4. Advanced sarcomere maturation in *Rhau* mutant mice. *A–D*, IF staining to display the thin filament in sagittal heart sections at E12.5 and E14.5. Thin filaments were stained by α-actinin (in *white*). The scale bars represent 10 μm. *E–L*, transmission electron microscopy of sarcomere structures of the cardiomyocytes from E12.5 and E14.5 embryos. The scale bars represent 2.5 μm. *M* and *N*, quantification of the sarcomere length in trabecular and compact zone at E12.5 and E14.5. Control mice: E12.5 (N = 3) and E14.5 (N = 4). *Rhau*$^{f/f}$*;cTNT-Cre* mice: E12.5 (N = 3) and E14.5 (N = 4). $p > 0.05$ (ns), $p < 0.01$ (**), $p < 0.001$ (***), and $p < 0.0001$ (****). *O* and *P*, quantification of the sarcomere thickness in trabecular and compact zone at E12.5 and E14.5. Control mice: E12.5 (N = 3) and E14.5 (N = 4). *Rhau*$^{f/f}$*;cTNT-Cre* mice: E12.5 (N = 3) and E14.5 (N = 4). $p > 0.05$ (ns), $p < 0.05$ (*), $p < 0.01$ (**), and $p < 0.0001$ (****). Control mice were *Rhau*$^{f/f}$ or *Rhau*$^{f/+}$ littermates. IF, immunofluorescence.

thoroughly studied for post-transcriptional regulation in our previous reports. We found that RHAU bound and resolved the G4 structure in the 5′-UTR of *Nkx2-5* mRNA for translation, and RHAU association with the 3′-UTR of *Nkx2-5* mRNA promoted the mRNA degradation. Accordingly, RHAU deficiency resulted in substantially increased level of *Nkx2-5* mRNA that could not be translated because of inhibitory effects of the G4 structure in its 5′-UTR, leading to remarkably reduced NKX2-5 protein level (20). Here, we disclosed a similar pattern of significantly enhanced *Nkx2-5* mRNA level but greatly reduced NKX2-5 protein level in the heart of *Rhau*$^{f/f}$*;cTNT-Cre* mice (Fig. 5, *B* and *C*), declaring a post-transcriptional regulation of *Nkx2-5* mRNA by RHAU. In addition, we found that *Hey2* exhibited a much higher mRNA level in the *Rhau* mutant heart than in control, but its protein level was markedly lower in the ventricular compact zone of *Rhau* mutant mice than control (Figs. 5, *D* and *F* and S4*A*). A G4-forming sequence was identified in the 5′-UTR of *Hey2* mRNA (Fig. 5*G*). The G4-forming fragment was inserted upstream of *GFP* coding sequence (Hey2-5′UTR-pEGFPN1), and it suppressed GFP translation (Fig. S4, *B* and *C*), and overexpression of *Rhau* substantially enhances GFP translation (Fig. S4, *D* and *E*). In the meantime, the cells transfected with G4 mutant vectors (G to A, Hey2-5′UTR-G4mut-pEGFPN1) showed comparable GFP expression level to the control group (Fig. S4, *B* and *C*), and overexpression of *Rhau* did not affect GFP translation anymore (Fig. S4, *F* and *G*). These data verified that RHAU modulated the *Nkx2-5* and *Hey2* mRNA through the post-transcriptional regulatory mechanism and identified *Hey2* mRNA as a new regulatory target of RHAU.

Defective myofibrillogenesis (sarcomere assembly) was proposed as a key pathogenic factor for NCC because mutation of the sarcomere genes was frequently identified in NCC patients. Therefore, we paid special attention to the sarcomere genes and noticed a considerable change of *Myh6* and *Myh7* mRNA level (Fig. 5*A*). Quantitative PCR (qPCR) and Western blot confirmed reduced *Myh7* mRNA and MYH7 protein level but enhanced *Myh6* mRNA and MYH6 protein level at different developmental stages (Fig. 5, *H–L*). These results revealed a switch from fetal form of MYH7 to adult form of MYH6 in the heart of *Rhau*$^{f/f}$*;cTNT-Cre* mice. BRG1 was reported to regulate the *Myh6/7* expression, but we did not detect a change of BRG1 protein level in the heart of *Rhau*$^{f/f}$*;cTNT-Cre* mice (Fig. 5, *K* and *L*).

RHAU regulated the expression of Myh7 *via its DNA resolvase activity*

The concordantly altered mRNA and protein levels of *Myh6/7* suggested that RHAU might regulate the transcription

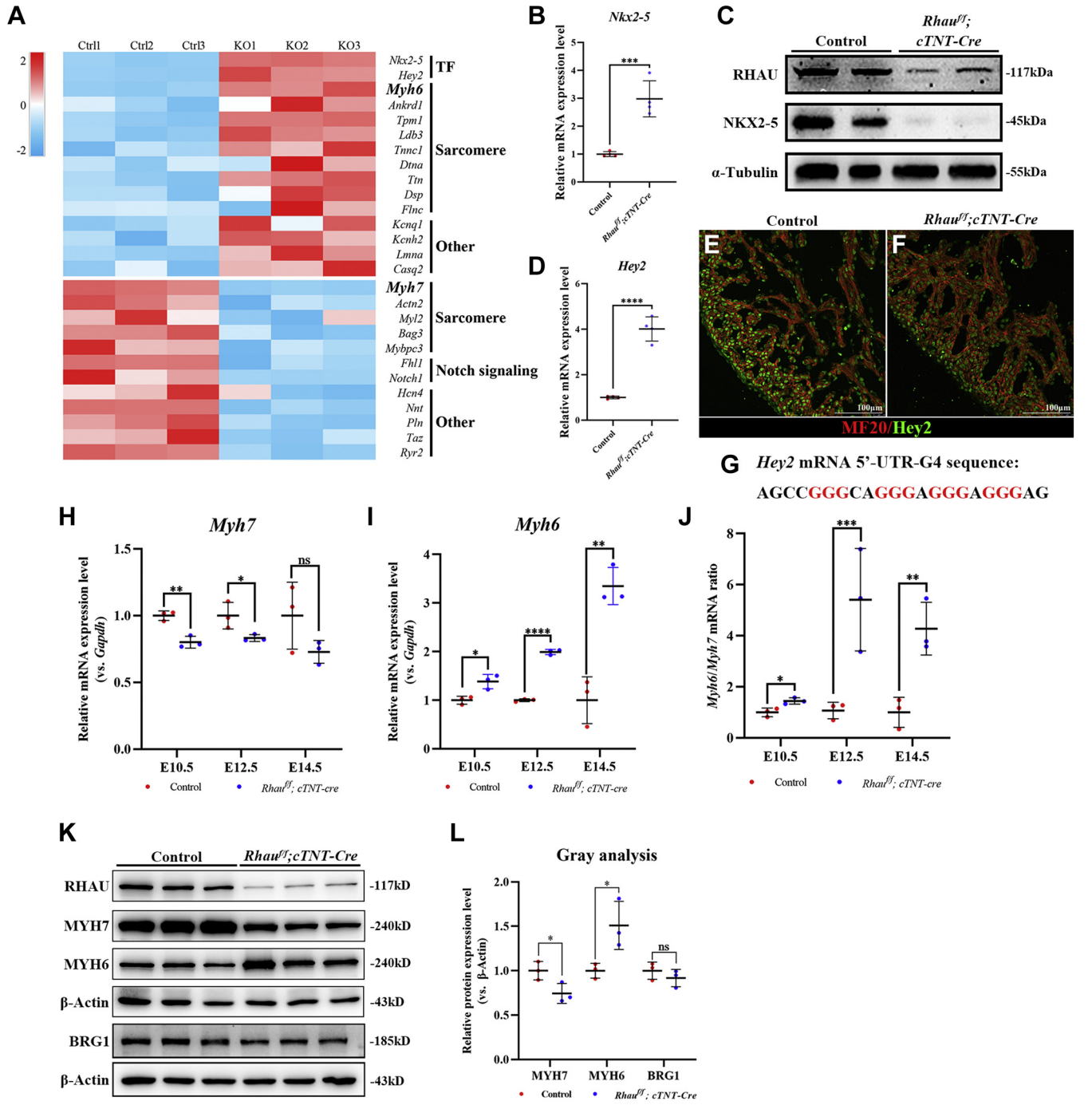

Figure 5. Altered expression pattern of NCC-associated genes in *Rhau* mutant heart. *A*, heat map showed the upregulated and downregulated genes associated with NCC in *Rhau* mutant mice at E15.5. *B* and *C*, quantitative RT–PCR and Western blot analysis for *Nkx2-5* mRNA and NKX2-5 protein in the heart from E14.5 embryos. N = 4 for control mice and N = 4 for *Rhau*$^{f/f}$*;cTNT-Cre* mice. $p < 0.001$ (***). *D*, quantitative RT–PCR for *Hey2* mRNA expression level in the heart from E14.5 mice. N = 4 for control mice and N = 4 for *Rhau*$^{f/f}$*;cTNT-Cre* mice. $p < 0.0001$ (****). *E* and *F*, IF staining for Hey2 in sagittal heart sections at E14.5. Cardiomyocytes were stained by MF20 (in *red*) and Hey2 (in *green*). Hey2 was abundant in the cardiomyocytes of compact zone, and an obvious reduced amount of Hey2 was shown in the *Rhau* mutant heart. The scale bars represent 100 μm. *G*, the predicted G4 sequence in the 5′-UTR of *Hey2* mRNA. *H* and *I*, quantitative RT–PCR of ventricular *Myh7* and *Myh6* expression levels at E10.5, E12.5, and E14.5. Control mice: E10.5 (N = 3), E12.5 (N = 3), and E14.5 (N = 3). *Rhau*$^{f/f}$*;cTNT-Cre* mice: E10.5 (N = 3), E12.5 (N = 3), and E14.5 (N = 3). $p > 0.05$ (ns), $p < 0.05$ (*), $p < 0.01$ (**), and $p < 0.0001$ (****). *J*, ratio of *Myh6*/*Myh7* mRNA. A switch from fetal *Myh7* to adult *Myh6* was remarkable. Control mice: E10.5 (N = 3), E12.5 (N = 3), and E14.5 (N = 3). *Rhau*$^{f/f}$*;cTNT-Cre* mice: E10.5 (N = 3), E12.5 (N = 3), and E14.5 (N = 3). $p < 0.05$ (*), $p < 0.01$ (**), and $p < 0.001$ (***). *K*, Western blot analysis of RHAU, MYH7, MYH6, and BRG1 in the heart of control and *Rhau* mutant mice at E14.5. *L*, quantification of (*K*). N = 3 for control mice and N = 3 for *Rhau*$^{f/f}$*;cTNT-Cre* mice. $p > 0.05$ (ns), $p < 0.05$ (*). Control mice were *Rhau*$^{f/f}$ or *Rhau*$^{f/+}$ littermates. IF, immunofluorescence; NCC, noncompaction cardiomyopathy; RHAU, RNA helicase associated with AU-rich element; TF, transcription factor.

of these genes through DNA G4 resolvase activity. We first checked whether there were G4 structures in the promoter region of these genes using QGRS mapper, a program to predict potential G4s in the DNA sequence (27), and the analysis uncovered three G4-forming sequences (termed G4-1, G4-2, and G4-3) in the promoter region of the *Myh7* genome (Fig. S5*A*). Next, we ordered synthesized DNA fragments based on these G4-forming sequences and performed *in vitro* G4 structure assay using G4-specific ligands of *N*-methyl mesoporphyrin IX (NMM) and thioflavin T (ThT) (28, 29). Upon the ligand binding to G4 DNA sequence, it would turn on the fluorescence, and the assay showed dramatically enhanced fluorescence intensity of NMM and ThT (Fig. S5, *B* and *C*). Thermal difference spectra and CD spectra exhibited typical profiles of G4 for G4-1, G4-2, and G4-3 fragments (Fig. S5, *D* and *E*). The CD profiles revealed that the G4-1 and G4-3 DNA fragments formed parallel-stranded G4, whereas the G4-2 DNA fragment formed a hybrid quadruplex structure (Fig. S5*E*). Furthermore, the thermal melting assays showed that these three DNA G4 structures were relatively stable (Fig. S5*F*). These data indicated potential G4 structures in the promoter region of the *Myh7* gene.

Afterward, we performed CUT&Tag-Seq, a new generation of ChIP-Seq with high repeatability and fine signal-to-noise ratio, by use of cardiomyocytes from control mice at E14.5 and RHAU antibody. Data from the CUT&Tag-Seq showed that the sites for RHAU binding were predominantly distributed near the transcription start sites (Fig. 6*A*), and motif analysis of these RHAU-binding regions revealed that majority of these motifs were G-enriched sequences (Fig. 6*B*). Peak calling analysis identified several peaks in the genome of *Myh7*, and one of them was located at the promoter region (Fig. 6*C*).

To examine whether RHAU regulated the expression of *Myh7* through resolving the DNA G4 structures in promoter region, we constructed enhanced GFP (EGFP)-derived reporters containing the G4-1 and G4-2 sequences (G4-1/2-pEGFPN1) and G4-3 sequence (G4-3-pEGFPN1). We transfected these reporters into 293T cells and collected cells after 72 h. Western blotting showed that the GFP protein level in the cells transfected with G4-1/2-pEGFPN1 and G4-3-pEGFPN1 were dramatically reduced compared with control (transfected with pEGFPN1) (Fig. S6*A*), indicating that the G4 sequences in the *Myh7* promoter region could suppress GFP expression. Then, we cotransfected mouse RHAU (*mRhau*-pCMV7.1) and G4-1/2-pEGFPN1 or G4-3-pEGFPN1 to the cells for detection of the protein and mRNA levels of GFP. We found that overexpression of RHAU improved the GFP expression level (Fig. 6, *D*–*I*). Multimutation of G to A in the

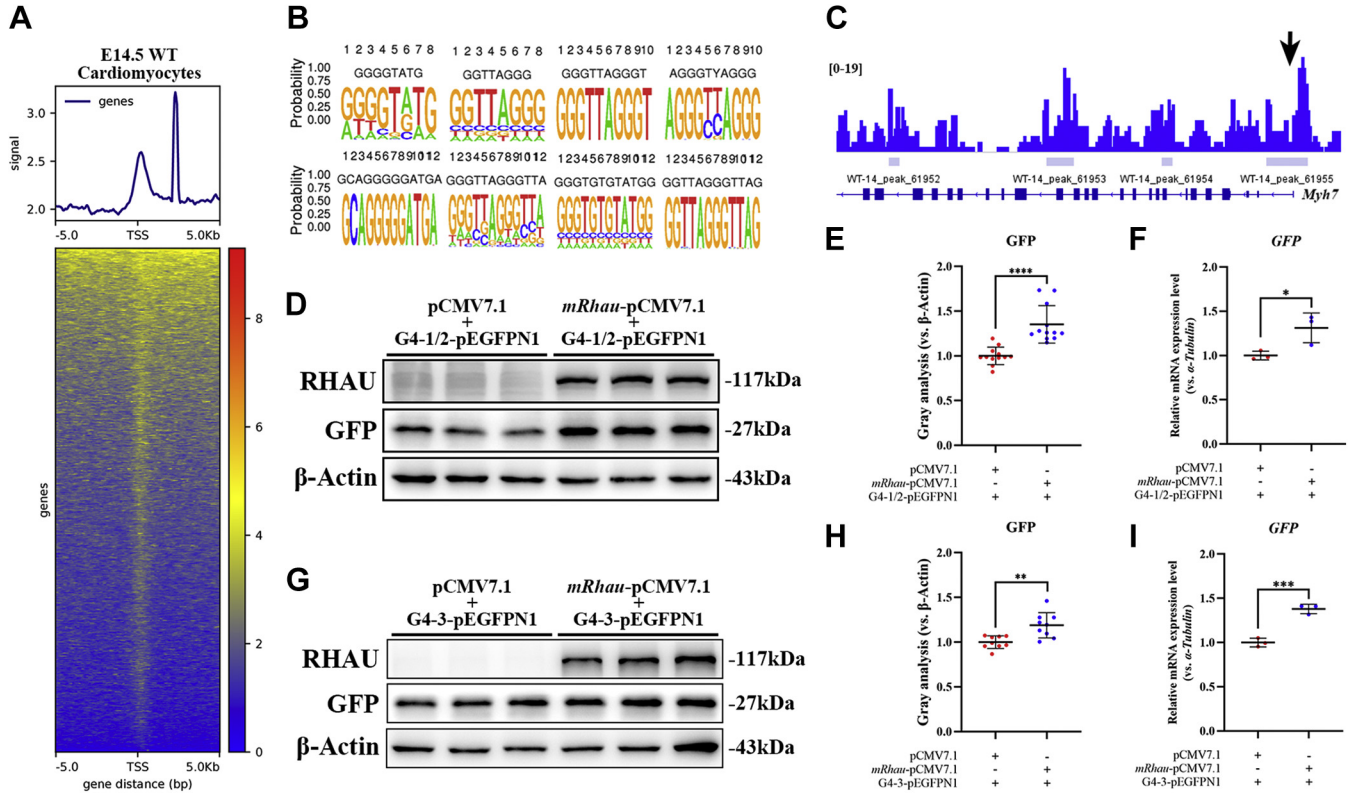

Figure 6. RHAU regulated the expression of *Myh7 via* its DNA resolvase activity. *A*, transcription start site (TSS) analysis of RHAU-binding sequences. *B*, RHAU-binding motifs. *C*, peak calling analysis showed RHAU could bind to the promoter of *Myh7*. *Black arrow* indicated the RHAU-binding peak that was positioned in the *Myh7* promoter. *D*, Western blot analysis of GFP expression level with or without RHAU overexpression in 293T cells. *E*, quantification of (*D*). N = 12 for control group and N = 12 for *Rhau* overexpression group. $p < 0.0001$ (****). *F*, quantitative RT–PCR of *GFP* mRNA expression level with or without RHAU overexpression in 293T cells. N = 3 for control group and N = 3 for *Rhau* overexpression group. $p < 0.05$ (*). *G*, Western blot analysis of GFP expression level with or without RHAU overexpression in 293T cells. *H*, quantification of (*G*). N = 9 for control group and N = 9 for *Rhau* overexpression group. $p < 0.01$ (**). *I*, quantitative RT–PCR of *GFP* mRNA expression level with or without RHAU overexpression in 293T cells. N = 3 for control group and N = 3 for *Rhau* overexpression group. $p < 0.001$ (***). RHAU, RNA helicase associated with AU-rich element.

G4 sequences of G4-1/2-pEGFPN1 and G4-3-pEGFPN1 reporters was generated, and the mutated reporters were used to transfect cells. Afterward, RHAU could no longer elevate the GFP expression level (Fig. S6, *B–E*).

One of the hallmarks of stress-induced cardiac pathological remodeling is the upregulation of *Myh7* mRNA and protein levels. Our recent study showed that *Rhau* knockout impaired neonatal heart regeneration in mice (21). To investigate whether RHAU regulates *Myh7* expression in postnatal heart regeneration, we performed a myocardial infarction (MI) surgery on control and *Rhau*$^{f/f}$;*α-MHC-Cre* mice at P5 and collected heart tissues at P19 for analysis of MYH7 protein level. In the control mice, MI injury robustly induced the expression of *Myh7* in the infarct zone (I) (Fig. S7). However, this kind of induction of *Myh7* was greatly suppressed in the *Rhau*$^{f/f}$;*α-MHC-Cre* mice.

Put together, these data demonstrated that RHAU facilitated transcription of *Myh7* by unwinding the G4 structures in the *Myh7* promoter.

Discussion

In this study, we investigated the function of the G4 resolvase RHAU in ventricular chamber development through deletion of *Rhau* in ventricular cardiomyocytes of mice, which reliably recapitulated human NCC.

Our mouse model supports the concept that defective myofibrillogenesis and sarcomere assembly are key pathogenic elements for NCC. Advanced sarcomere structure and disrupted MYH6/7 protein level were observed in the RHAU-deficient mice. The isoform switch of MYH protein from fetal MYH7 to adult MYH6 was generated ahead of developmental stage and might trigger pathological remodeling of embryonic myocardium, leading to abnormal trabeculation and compaction. The advanced sarcomere assembly was possibly a consequence of earlier MYH7 to MYH6 switch that was programmed after birth during normal developmental process.

Our previous studies elucidated the function of RHAU in post-transcriptional regulation of gene expression *via* binding to mRNA. Here, we uncovered that RHAU could also modulate gene expression at transcriptional level through its DNA G4 resolvase activity and identified *Myh7* as a regulatory target of RHAU. RHAU facilitated the transcription of *Myh7*, and in the absence of RHAU, a switch from *Myh7* to *Myh6* was provoked, suggesting that suppression of *Myh7* could activate the transcription of *Myh6*. This finding added to our knowledge toward the regulation of *Myh6/7* expression by BRG1. The *Myh7* gene is located in tandem with the *Myh6* gene, and numerous studies uncovered the intriguing phenomena that the expression level of these two genes often shows an opposite change. For instance, the expression level of *Myh7* was greatly enhanced, whereas that of *Myh6* was substantially suppressed during pathological heart remodeling.

Mutations of *Myh6*, *Myh7*, *Nkx2-5*, and *Hey2* were found in several forms of cardiomyopathies, including NCC, hypertrophic, and dilated cardiomyopathy. How mutations in the same panel of genes cause enormously distinct clinical phenotypes is puzzling. In a recent publication, Dr Srivastava *et al.* reported NKX2-5 variant as a genetic modifier in conjunction with the sarcomere MYH7 mutant and a transcription factor MKL2 mutant contributing to NCC, which helps understand this study. We detected a substantial reduction of NKX2-5 protein level in the RHAU mutant heart. Reduced NKX2-5 together with MYH isoform switch from MYH7 to MYH6 might triggered trabecular pathological remodeling, whereas NKX2-5 reduction in combination with decreased Hey2 level impaired compaction, leading to thinned ventricular wall. On the other hand, our study demonstrated that disrupted expression level, in addition to mutation, of these genes was pathogenic for NCC.

The contribution of cardiomyocyte proliferation to NCC is of debate. Our finding of reduced cardiomyocyte proliferation in the RHAU mutant mice suggests that poor cardiomyocyte mitosis was one of the driving factors for NCC.

In summary, our findings unveiled the synergistic effects of altered protein levels of NKX2-5, MYH6/7, and Hey2 in the pathogenesis of NCC. Especially, the fetal MYH7 to adult MYH6 switch-elicited pathological remodeling might contribute hugely to NCC (Fig. 7). Some of the RHAU mutant mice reported in this study could survive to 2 months, which makes this mouse model particularly useful to understand NCC.

Experimental procedures

Mice

Mouse strains used in this study are previously reported: *Rhau* floxed mice (20, 21); *Mef2c-AHF-Cre* mice (22); *cTNT-Cre* mice (23); *Tie2-Cre* mice (30); and *α-MHC-Cre* mice (31). Genotyping of these mice was as reported before. All mouse strains were maintained on C57BL/6 genetic background. Mice were group-housed in accordance with the regulations on mouse welfare and ethics of Nanjing University, with 12 h/12 h light–dark cycles and had *ad libitum* access to food and water. The Institutional Animal Care and Use Committee of Model Animal Research Center of Nanjing University approved all animal procedures used in this study. Control mice used in this study were usually *Rhau*$^{f/f}$ littermates.

Western blotting analysis

Embryonic heart tissues were collected, snap frozen in liquid nitrogen, and then stored at −80 °C until use. Heart tissue lysates were prepared in radioimmunoprecipitation assay buffer (Beyotime Biotechnology; P0013B) with PMSF. To prepare cell lysates, the culture medium was discarded and the cells were washed with PBS. Afterward, radioimmunoprecipitation assay was added to the cells, and the cells were collected for centrifugation at 4 °C for 15 min. The heart tissue and cell lysate samples were resolved by 10% SDS-PAGE gels and transferred onto polyvinylidene fluoride membranes (Millipore). The membranes were blocked with 5% bovine serum albumin in Tris-buffered saline with Tween-20 for 1 h at room temperature and were then

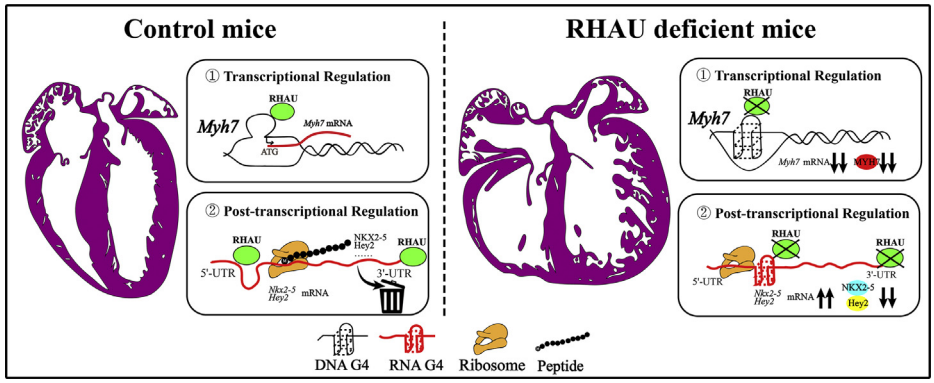

Figure 7. Working model of RHAU regulation of ventricular chamber development and RHAU deficiency–elicited NCC. *Left panel* (control mice), RHAU regulated gene expression through transcriptional (*Myh7*) and post-transcriptional (*Nkx2-5* and *Hey2*) mechanisms. The G4 structures in the promoter region of *Myh7* and the 5′-UTRs of *Nkx2-5* and *Hey2* mRNA could be resolved by RHAU for transcription and translation. *Right panel* (RHAU-deficient mice), under conditions of RHAU deficiency, mRNA levels of *Nkx2-5* and *Hey2* were markedly elevated, but their protein level was profoundly reduced. Meanwhile, the transcription of *Myh7* was decreased leading to reduced MYH7 but enhanced MYH6 protein level. A synergistic effect of altered protein levels of NKX2-5, MYH6/7, and Hey2 in the pathogenesis of NCC was proposed. Especially, the fetal MYH7 to adult MYH6 switch-elicited pathological remodeling might contribute hugely to NCC. NCC, noncompaction cardiomyopathy; RHAU, RNA helicase associated with AU-rich element.

incubated with primary antibodies overnight at 4 °C. The next day, membranes were washed with Tris-buffered saline with Tween-20 and incubated with a secondary antibody for 2 h at room temperature. The results were visualized with the Tanon-5200 imaging system (Tanon). The antibodies are listed in Table S1.

RNA-Seq and RT–qPCR

Heart ventricles were dissected from control and *Rhau*$^{f/f}$;*cTNT-Cre* mice at E13.5 and E15.5. Total RNA was extracted from these tissues using TRIzol Reagent (Life Technologies; 15596018) following the manufacturer's instructions. RNA-Seq was conducted by Vazyme Biotech. The RNA integrity was accurately detected using the Agilent 2100. After library construction, sequencing, and other steps, raw reads (150 bp read length) of corresponding samples were obtained. The reference sequences of the corresponding species downloaded from the National Center for Biotechnology Information, University of California, Santa Cruz, Ensemble, and other databases were used for biological information analysis. The expected number of Fragments Per Kilobase of transcript sequence per Millions base pairs sequenced was used to show gene expression level. The cuffDiff analysis module of CuffLinks was used to analyze gene differential expression between samples.

For qPCR, reverse transcription was performed using a HiScript II Q Select RT Supermix for qPCR (+gDNA wiper) kit (Vazyme Biotech; R223-01), and the products were applied to qPCR using an AceQ Universal SYBR Master Mix Kit (Vazyme Biotech; Q511-02) and an ABI QuantStudio 5. Data were normalized to control value as one, and the fold changes were presented. The primers for qPCR were provided in Table S2.

Plasmid construction

5′-UTR (135 bp) of *Hey2* was amplified *via* PCR from mice genomic DNA and inserted into the pEGFPN1 vectors to generate Hey2-5′UTR-pEGFPN1 constructs. Two 320 bp fragments containing the three G4s (one with G4-1/2 sequence and the other with G4-3 sequence) of the mouse *Myh7* were amplified *via* PCR from mice genomic DNA and subsequently cloned into the pEGFPN1 vectors to generate G4-1/2-pEGFPN1 and G4-3-pEGFPN1 constructs.

Hey2-5′UTR-pEGFPN1 was used as template to generate the mutant form of Hey2-5′UTR-G4mut-pEGFPN1 plasmids by PCR with 5′- and 3′- complementary primers containing the mutation sequence (GGG to GAG). PCR was carried out using the 5′- and 3′- complementary primers for 35 cycles, respectively. Then, the two PCR products were denatured at 95 °C for 5 min and annealed at room temperature overnight. The next day, Dpn I (11001ES) was added to destroy the template DNA, and the products were used to transform competent cells (C502-02). Single colonies were picked up for sequencing. G4-1/2mut-pEGFPN1 and G4-3mut-pEGFPN1 plasmids were obtained by the same method. The primers for plasmid construction are listed in Table S3.

Cell culture and transfection

Human embryonic kidney 293T cells were maintained in Dulbecco's modified Eagle's medium, supplemented with 10% fetal calf serum and 1% penicillin–streptomycin, in the presence of 5% CO_2 at 37 °C incubators. Transient transfection was performed using Lipofectamine 2000 (Life Technologies; 11668-027) following the manufacturer's instructions. Fresh medium was added to the cells 4 to 6 h after transfection. The cells were collected 48 to 72 h after transfection for further analysis. The siRNA sequences were showed in Table S4.

Histological and IF staining analysis

Hearts were dissected and fixed in 4% paraformaldehyde overnight at 4 °C. The samples were dehydrated (30% ethanol, 50% ethanol, 75% ethanol, 85% ethanol, 95% ethanol twice, and butanol three times) and embedded in paraffin. For H&E staining, 8 μm sections were prepared.

For IF staining, hearts were dissected and fixed in 4% paraformaldehyde overnight at 4 °C, then rinsed in PBS for three times, and incubated in 30% sucrose at 4 °C overnight. Afterward, the heart samples were embedded in optical coherence tomography and stored at −20 °C for frozen sections (10 μm). For staining, the frozen sections were rinsed three times in PBS and blocked in goat serum for 1 h at room temperature. Then, sections were incubated with primary antibodies overnight at 4 °C and washed in PBS and incubated with secondary antibodies for 2 h at room temperature. Primary antibodies were listed in Table S2. IF staining for TUNEL assay was carried out using standard protocols (Vazyme Biotech; A113-01). Imaging were processed with Leica SP5 laser confocal microscope and Olympus FV3000 microscope.

Cardiomyocytes isolation and CUT&Tag assay

E14.5 cardiac ventricles were harvested and finely chopped to 1 to 2 mm^3. Then these tissues were transferred into 15 ml centrifuge tube, and the enzyme buffer (0.1% trypsin and 0.25% collagenase type II) was added. The centrifuge tube was constantly shaken in a 37 °C water bath to digest the cardiac tissues. Fetal bovine serum was added 10 to 15 min later to terminate digestion, and the supernatant was collected and centrifuged. The enzyme buffer was added back into the tissue containing tubes for further digestion. Then, these procedures were repeated three and four times until no visible myocardial tissue was observed. The harvested cardiac cells were seeded into cell dishes. About 2 to 3 h later, the supernatant was transferred into centrifuge tube (differential attachment techniques) for further experiment.

Isolated cardiomyocytes were used for the CUT&Tag assay. CUT&Tag assay were processed according to the manufacturer's protocol (TD901-02; Vazyme). And the libraries were generated using TruePrep Index Kit V2 for Illumina (TD202; Vazyme). CUT&Tag analysis was performed as previously described (32).

MI surgery

MI surgery was performed as previously described (21). Briefly, MI surgery was performed in control and *Rhau*$^{f/f}$;*α-MHC-Cre* mice at P5. The mice were placed on ice for 3 to 5 min until they are unconscious. Cut the skin of mice with microscissors, and blunt separation was performed between the third and fourth ribs. The left anterior descending branch was ligated with a 10 to 0 suture, and then, the skin wound was closed. The whole procedure lasted within 10 min. After the operation, the mice were placed on a heating lamp at 37 °C until their body temperature and activity were restored. The mice were sacrificed 2 weeks after the MI surgery (P19) for Western blot analysis.

Spectroscopy measurement and NMM/ThT fluorescence spectrum

Preparation of DNA solution: oligonucleotide was diluted to 5 μM in a 10 mM Tris–HCl buffer containing 50 mM KCl at pH 7.0. The DNA solution was heated at 95 °C for 5 min, then slowly cooled to room temperature, and then stored at 4 °C for the subsequent experiment.

The fluorescent ligand NMM/ThT can specifically bind to the G4 structures, thereby limiting the rotation of the fluorescent molecules and enhancing the fluorescence intensity. The NMM/ThT fluorescence experiment was measured by the FS980 fluorescence spectrometer (Edinburgh Technologies Ltd). The samples (10 μM NMM/ThT and 1 μM oligonucleotides in 10 mM Tris–HCl buffer, pH 7.0) were measured at excitation wavelength of 440 nm, emission wavelength of 475 to 570 nm, slit of 5 nm, photo multiplier tube of 600 V, and 25 °C.

The thermal difference spectra were performed on a Cary 100UV/VIS spectrophotometer (Agilent Technologies). Absorption spectra were recorded in the range of 220 to 350 nm at the scanning speed of 600 nm/min and data interval of 1 nm at both temperatures.

The CD spectrum was recorded by Chirascan (Applied Optical Physics), and the scanning speed is 2 nm/s, and the scanning wavelength ranges from 220 to 350 nm at 25 °C.

Ultraviolet melting was measured using a Cary 100 UV/Visible Spectrophotometer (Agilent Technologies), and the absorbance at 295 nm was recorded. The temperature range was 5 to 95 °C, and the temperature gradient was 0.5 °C/min.

Statistical analysis

All data analyses were performed with GraphPad Prism software, version 8.0 (GraphPad Software). ImageJ (National Institutes of Health) was applied for quantification study. Statistical comparisons were carried out using the two-tailed Student's t tests. A value of $p < 0.05$ (*) was considered statistically significant; $p < 0.01$ (**), $p < 0.001$ (***), and $p < 0.0001$ (****) were considered very statistically significant. ns represented no significant difference. In all the figures, measurements were reported as the mean ± SD. Please see Table S5 for a list of abbreviations.

Data availability

All data are available in the main article or the supporting information.

Supporting information—This article contains supporting information.

Acknowledgments—We thank Dr Bin Zhou (Albert Einstein College of Medicine, New York) for providing the *cTNT-Cre* mice.

Author contributions—X. H. and Z. Y. conceptualization; M. J. and J. Z. methodology; X. H., K. Z., and D. Q. investigation; X. H. writing–original draft; J. Z. and Z. Y. writing–review & editing; J. Z. and Z. Y. supervision.

Funding and additional information—This work was supported by grants from the National Key Research and Development Program of China (grant no.: 2019YFA0801601) and grants from the National Natural Science Foundation of China (grant nos.: 31930029, 91854111, and 31571490) (to Z. Y.).

Conflict of interest—The authors declare that they have no conflicts of interest with the contents of this article.

Abbreviations—The abbreviations used are: EGFP, enhanced GFP; G4, G-quadruplex; IF, immunofluorescence; LV, left ventricle; MI, myocardial infarction; NCC, noncompaction cardiomyopathy; NMM, *N*-methyl mesoporphyrin IX; qPCR, quantitative PCR; RHAU, RNA helicase associated with AU-rich element; RV, right ventricle; ThT, thioflavin T.

References

1. Oechslin, E., Jenni, R., and Klaassen, S. (2020) Left ventricular non-compaction is a myocardial phenotype: Cardiomyopathy-yes or no? *Can. J. Cardiol.* **37**, 366–369
2. Towbin, J. A., Lorts, A., and Jefferies, J. L. (2015) Left ventricular non-compaction cardiomyopathy. *Lancet* **386**, 813–825
3. Jefferies, J. L. (2021) Left ventricular noncompaction cardiomyopathy: New clues in a not so new disease? *J. Am. Heart Assoc.* **10**, e018815
4. Liu, Y., Chen, H., and Shou, W. (2018) Potential common pathogenic pathways for the left ventricular noncompaction cardiomyopathy (LVNC). *Pediatr. Cardiol.* **39**, 1099–1106
5. Choquet, C., Kelly, R. G., and Miquerol, L. (2019) Defects in trabecular development contribute to left ventricular noncompaction. *Pediatr. Cardiol.* **40**, 1331–1338
6. Chen, H., Zhang, W., Li, D., Cordes, T. M., Mark Payne, R., and Shou, W. (2009) Analysis of ventricular hypertrabeculation and non-compaction using genetically engineered mouse models. *Pediatr. Cardiol.* **30**, 626–634
7. Tian, X., Li, Y., He, L., Zhang, H., Huang, X., Liu, Q., Pu, W., Zhang, L., Li, Y., Zhao, H., Wang, Z., Zhu, J., Nie, Y., Hu, S., Sedmera, D., *et al.* (2017) Identification of a hybrid myocardial zone in the mammalian heart after birth. *Nat. Commun.* **8**, 87
8. Yue, Y., Zong, W., Li, X., Li, J., Zhang, Y., Wu, R., Liu, Y., Cui, J., Wang, Q., Bian, Y., Yu, X., Liu, Y., Tan, G., Zhang, Y., Zhao, G., *et al.* (2020) Long-term, in toto live imaging of cardiomyocyte behaviour during mouse ventricle chamber formation at single-cell resolution. *Nat. Cell Biol.* **22**, 332–340
9. Luxán, G., D'Amato, G., MacGrogan, D., and de la Pompa, J. L. (2016) Endocardial Notch signaling in cardiac development and disease. *Circ. Res.* **118**, e1–e18
10. D'Amato, G., Luxán, G., and de la Pompa, J. L. (2016) Notch signalling in ventricular chamber development and cardiomyopathy. *FEBS J.* **283**, 4223–4237
11. Luxán, G., Casanova, J. C., Martínez-Poveda, B., Prados, B., D'Amato, G., MacGrogan, D., Gonzalez-Rajal, A., Dobarro, D., Torroja, C., Martinez, F., Izquierdo-García, J. L., Fernández-Friera, L., Sabater-Molina, M., Kong, Y. Y., Pizarro, G., *et al.* (2013) Mutations in the NOTCH pathway regulator MIB1 cause left ventricular noncompaction cardiomyopathy. *Nat. Med.* **19**, 193–201
12. Oechslin, E., and Jenni, R. (2017) Nosology of noncompaction cardiomyopathy: The emperor still wears clothes! *Can. J. Cardiol.* **33**, 701–704
13. Richard, P., Ader, F., Roux, M., Donal, E., Eicher, J. C., Aoutil, N., Huttin, O., Selton-Suty, C., Coisne, D., Jondeau, G., Damy, T., Mansencal, N., Casalta, A. C., Michel, N., Haentjens, J., *et al.* (2019) Targeted panel sequencing in adult patients with left ventricular non-compaction reveals a large genetic heterogeneity. *Clin. Genet.* **95**, 356–367
14. Gifford, C. A., Ranade, S. S., Samarakoon, R., Salunga, H. T., de Soysa, T. Y., Huang, Y., Zhou, P., Elfenbein, A., Wyman, S. K., Bui, Y. K., Cordes Metzler, K. R., Ursell, P., Ivey, K. N., and Srivastava, D. (2019) Oligogenic inheritance of a human heart disease involving a genetic modifier. *Science* **364**, 865–870
15. Sauer, M., and Paeschke, K. (2017) G-quadruplex unwinding helicases and their function *in vivo*. *Biochem. Soc. Trans.* **45**, 1173–1182
16. Varshney, D., Spiegel, J., Zyner, K., Tannahill, D., and Balasubramanian, S. (2020) The regulation and functions of DNA and RNA G-quadruplexes. *Nat. Rev. Mol. Cell Biol.* **21**, 459–474
17. Chen, M. C., Tippana, R., Demeshkina, N. A., Murat, P., Balasubramanian, S., Myong, S., and Ferré-D'Amaré, A. R. (2018) Structural basis of G-quadruplex unfolding by the DEAH/RHA helicase DHX36. *Nature* **558**, 465–469
18. Sauer, M., Juranek, S. A., Marks, J., De Magis, A., Kazemier, H. G., Hilbig, D., Benhalevy, D., Wang, X., Hafner, M., and Paeschke, K. (2019) DHX36 prevents the accumulation of translationally inactive mRNAs with G4-structures in untranslated regions. *Nat. Commun.* **10**, 2421
19. Tran, H., Schilling, M., Wirbelauer, C., Hess, D., and Nagamine, Y. (2004) Facilitation of mRNA deadenylation and decay by the exosome-bound, DExH protein RHAU. *Mol. Cell* **13**, 101–111
20. Nie, J., Jiang, M., Zhang, X., Tang, H., Jin, H., Huang, X., Yuan, B., Zhang, C., Lai, J. C., Nagamine, Y., Pan, D., Wang, W., and Yang, Z. (2015) Post-transcriptional regulation of Nkx2-5 by RHAU in heart development. *Cell Rep.* **13**, 723–732
21. Jiang, M., Hu, H., Zhao, K., Di, R., Huang, X., Shi, Y., Yue, Y., Nie, J., Yu, S., Wang, W., and Yang, Z. (2020) The G4 resolvase RHAU modulates mRNA translation and stability to sustain postnatal heart function and regeneration. *J. Biol. Chem.* **296**, 100080
22. Verzi, M. P., McCulley, D. J., De Val, S., Dodou, E., and Black, B. L. (2005) The right ventricle, outflow tract, and ventricular septum comprise a restricted expression domain within the secondary/anterior heart field. *Dev. Biol.* **287**, 134–145
23. Jiao, K., Kulessa, H., Tompkins, K., Zhou, Y., Batts, L., Baldwin, H. S., and Hogan, B. L. (2003) An essential role of Bmp4 in the atrioventricular septation of the mouse heart. *Genes Dev.* **17**, 2362–2367
24. Chen, H., Shi, S., Acosta, L., Li, W., Lu, J., Bao, S., Chen, Z., Yang, Z., Schneider, M. D., Chien, K. R., Conway, S. J., Yoder, M. C., Haneline, L. S., Franco, D., and Shou, W. (2004) BMP10 is essential for maintaining cardiac growth during murine cardiogenesis. *Development* **131**, 2219–2231
25. Pashmforoush, M., Lu, J. T., Chen, H., Amand, T. S., Kondo, R., Pradervand, S., Evans, S. M., Clark, B., Feramisco, J. R., Giles, W., Ho, S. Y., Benson, D. W., Silberbach, M., Shou, W., and Chien, K. R. (2004) Nkx2-5 pathways and congenital heart disease; loss of ventricular myocyte lineage specification leads to progressive cardiomyopathy and complete heart block. *Cell* **117**, 373–386
26. Guo, Y., and Pu, W. T. (2020) Cardiomyocyte maturation: New phase in development. *Circ. Res.* **126**, 1086–1106
27. Kikin, O., D'Antonio, L., and Bagga, P. S. (2006) QGRS mapper: A web-based server for predicting G-quadruplexes in nucleotide sequences. *Nucleic Acids Res.* **34**, W676–W682
28. Kreig, A., Calvert, J., Sanoica, J., Cullum, E., Tipanna, R., and Myong, S. (2015) G-quadruplex formation in double strand DNA probed by NMM and CV fluorescence. *Nucleic Acids Res.* **43**, 7961–7970
29. Xu, S., Li, Q., Xiang, J., Yang, Q., Sun, H., Guan, A., Wang, L., Liu, Y., Yu, L., Shi, Y., Chen, H., and Tang, Y. (2016) Thioflavin T as an efficient fluorescence sensor for selective recognition of RNA G-quadruplexes. *Sci. Rep.* **6**, 24793
30. Feng, Q., Di, R., Tao, F., Chang, Z., Lu, S., Fan, W., Shan, C., Li, X., and Yang, Z. (2010) PDK1 regulates vascular remodeling and promotes epithelial-mesenchymal transition in cardiac development. *Mol. Cell. Biol.* **30**, 3711–3721
31. Zhao, X., Lu, S., Nie, J., Hu, X., Luo, W., Wu, X., Liu, H., Feng, Q., Chang, Z., Liu, Y., Cao, Y., Sun, H., Li, X., Hu, Y., and Yang, Z. (2014) Phosphoinositide-dependent kinase 1 and mTORC2 synergistically maintain postnatal heart growth and heart function in mice. *Mol. Cell. Biol.* **34**, 1966–1975
32. Xu, M., Yao, J., Shi, Y., Yi, H., Zhao, W., Lin, X., and Yang, Z. (2021) The SRCAP chromatin remodeling complex promotes oxidative metabolism during prenatal heart development. *Development* **148**, dev199026